Communication

Machine-Learning-Based Generative Optimization Method and Its Application to an Antenna Decoupling Design

Hao Huang, Xue-Song Yang, and Bing-Zhong Wang

***Abstract*— A machine-learning-based generative optimization method using masked autoencoders (MAE) is proposed and applied to multi-objective antenna decoupling structure design. The machine learning method contains k-means algorithm and MAE neural network structure. The k-means is used for label-free classification of decoupling structure samples, and MAE is used for the intelligent optimization design of decoupling structures. By applying the machine-learning-based method, MAE optimization models for designing decoupling structures are obtained. An antenna decoupling example using neutralization line is selected to validate the effectiveness of the proposed optimization method. Measurement results show that the neutralization line designed by the proposed method improves the antenna isolation by at least 6 dB, that is, S_{21} reaches below at least −18 dB between 3.5 and 9.7 GHz, while requiring little manual intervention during the optimization progress.**

***Index Terms*— k-means clustering, machine learning, neutralization line, optimization method.**

I. Introduction

With the continuous development of wireless communication technology, people put forward higher requirements for the channel capacity and communication quality of wireless communication systems. Multiple-input-multiple-output (MIMO) technology provides a solution to these requirements by placing multiple antennas at transmitter and receiver, greatly increasing communication capacity. However, the dense arrangement of multiple antennas in a limited space can cause severe mutual coupling between elements and then deteriorate the performance. Thus, reducing mutual coupling between MIMO antenna elements is an important task in MIMO antenna design [1].

Many solutions have been proposed to reduce the mutual coupling [2], [3], [4], [5], [6], [7], [8], [9], [10], such as parasitic elements [2], [3], decoupling networks [4], [5], defected ground structures [6], [7], and so on [8], [9], [10]. Among these decoupling methods, neutralization line is an effective method which requires less space between antennas and achieves good performance [9], [10].

The traditional design method of neutralization line is based on a prior design experience and trials to determine the general shape of decoupling structure and then optimize its geometrical parameters. In recent years, some intelligent optimization algorithms have gradually been used in the field of electromagnetic design [11], [12], [13], [14], and the machine-learning-based methods are particularly noteworthy among them. With its wide application, many researchers are studying machine-learning-assisted optimization and design methods for electromagnetic problems, such as antenna or filter design, inverse scattering problem solving, and so on [15], [16], [17], [18], [19], [20], [21], [22]. For example, building neural network antenna models to replace the simulation process [15], [16], [17], [18], designing inverse models to predict the values of design variables [19], and accelerating the solution of integral equation [20], [21], [22]. However, these machine-learning-assisted methods have major application limitations, such as the inability to change the basic shape of the electromagnetic structure, the inability to output design parameters outside the parameter range of the training sample set, and so on. Besides, most of the neural network-based models or methods only accomplish parametric electromagnetic modeling or optimization, and do not take full advantage of the powerful image-based mapping capabilities of the new neural networks.

In this communication, to further reduce the requirement of a priori knowledge for electromagnetic design engineers, while fully utilizing the generalization ability of the machine learning models, a novel neural network structure called masked autoencoders (MAE) is used to build the optimal model of an antenna decoupling structure. MAE is a new type of autoencoder. Like autoencoder in general, MAE is often used for computer vision tasks such as image reconstruction and image recognition due to its feature extraction capability. The k-means algorithm is used to classify the training samples of the MAE model without labels. To build MAE multiobjective optimization model, each objective is set as a classification feature of the k-means algorithm.

By combining the k-means algorithm with an MAE model, the optimization model of an antenna neutralization line is obtained. Measurement result shows that the designed neutralization line for ultra-wide band (UWB) antennas improves the antenna isolation by at least 6 dB, that is, S_{21} basically reaches below at least −18 dB within the operating frequency band, and the whole optimization process needs little manual intervention of the designer.

The organization of this communication is as follows. The basic methodological theory and modeling process are briefly presented in Section II, the validation of the proposed method and its performance are described in Section III, the measurement and comparison are given in Section IV, and the conclusion is given in Section V.

II. Machine-Learning-Based Optimization Methodology

A. MAE Model

MAE is a new type of autoencoder model [23]. It contains two subnetworks named encoder and decoder, respectively. Compared with the general autoencoder, the input of MAE's encoder network is incomplete image information, while the input of the decoder network is not only the output of the encoding network, but also the location

Manuscript received 19 September 2022; revised 7 April 2023; accepted 19 April 2023. Date of publication 1 May 2023; date of current version 7 July 2023. This work was supported by the National Natural Science Foundation of China under Grant 62271112. *(Corresponding author: Xue-Song Yang.)*

Hao Huang and Xue-Song Yang are with the School of Physics, University of Electronic Science and Technology of China, Chengdu 611731, China, and also with the Huzhou Key Laboratory of Terahertz Integrated Circuits and Systems, Huzhou 313000, China (e-mail: hao_huang@std.uestc.edu.cn; xsyang@uestc.edu.cn).

Bing-Zhong Wang is with the School of Physics, University of Electronic Science and Technology of China, Chengdu 611731, China (e-mail: bzwang@uestc.edu.cn).

Color versions of one or more figures in this communication are available at https://doi.org/10.1109/TAP.2023.3270716.

Digital Object Identifier 10.1109/TAP.2023.3270716

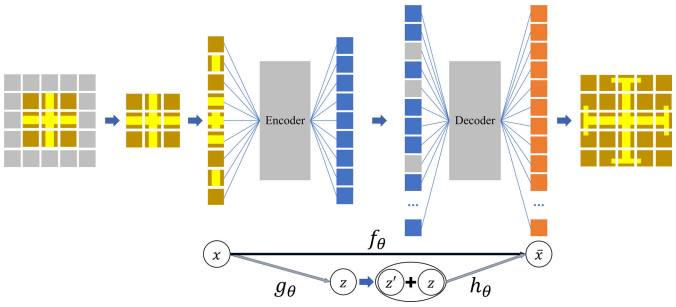

Fig. 1. Structure of MAE model.

token of the missing part of the image. The structure of MAE is shown in Fig. 1.

For a mapping relationship

$$f_\theta : x \to \bar{x} \tag{1}$$

the training of MAE model is divided into two parts

$$g_\theta : x \to z \tag{2}$$

$$h_\theta : z + z' \to \bar{x} \tag{3}$$

the encoder network learns the mapping relationship g_θ, it encodes the incomplete high-dimensional input x into the low-dimensional latent variable z (feature variable), which is a process of encoding the data; the decoder network learns the mapping relationship h_θ, it decodes the combination of the latent variable z and masked position token z' into the complete high-dimensional $\bar{x}$, which is a process of decoding the data. Due to this special mapping method, autoencoder is often used for image restoration [24], noise cancellation [25], and so on [26], [27].

In the process of image reconstruction, the role of encoder is to extract the feature covariates of an image and put them into the decoder. The role of decoder is to receive the output of the encoder, intentionally masked it with noise, and then restore the masked parts based on the received information. The MAE model initially masked the original image randomly. But in this method, we manually select the designed part of the decoupling structure as the masked area.

B. k-Means-Based Self-Supervised Classification of Samples

k-means algorithm is a basic unsupervised classification method, which takes the feature parameters of the instance as input and the category of that as output [28].

Given an unlabeled sample dataset D

$$D = \{x_1, x_2, \ldots, x_n\} \tag{4}$$

where x_i is the ith unlabeled sample, and each sample $x_i = \{x_{i1}, x_{i2}, \ldots, x_{im}\}$ is an m-dimensional feature vector. The k-means algorithm divides the sample set D into k disjoint clusters $\{C_l | l = 1, 2, \ldots, k\}$ based on the Euclidean distance, and each cluster contains a variable number of samples. Therefore, the classification result of the sample set D is denoted by the following equation:

$$P = \{C_1, C_2, \ldots, C_k\} \tag{5}$$

where

$$C_i \cap C_j = \emptyset, \quad i \neq j \tag{6}$$

$$C_1 \cup C_2 \cup \cdots \cup C_k = D. \tag{7}$$

To build MAE multiobjective optimization model, several parameters of antennas are used as feature parameters in classification, as shown in Fig. 2. Neutralization lines with similar decoupling performance are classified into the same class so that the designed MAE learns their commonality to generate high-performance structures based on them.

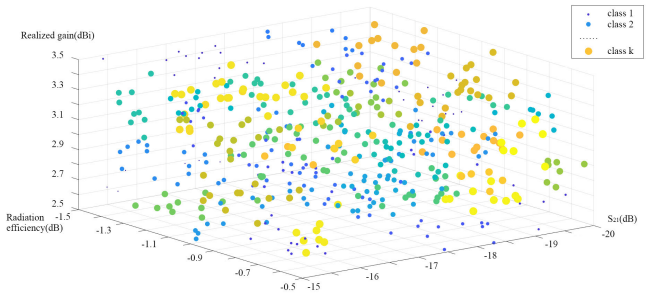

Fig. 2. Sample unlabeled classification based on k-means algorithm (three targets). A total of 3000 samples of two-element antennas with different neutralization lines were collected, and S-parameters, radiation efficiency, and realized gain of the antenna for optimized frequency points are used as feature parameters in classification. ($S_{21} \in [-20$ dB, -15 dB], radiation efficiency $\in [-1.5$ dB, -0.5 dB], and realized gain $\in$ [2.5 dBi, 3.5 dBi].)

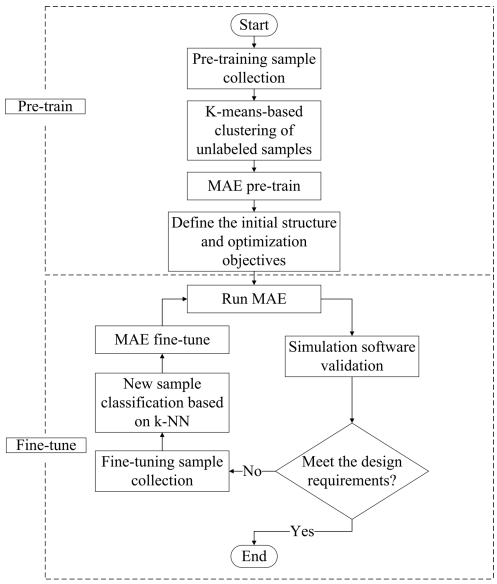

Fig. 3. Model training process.

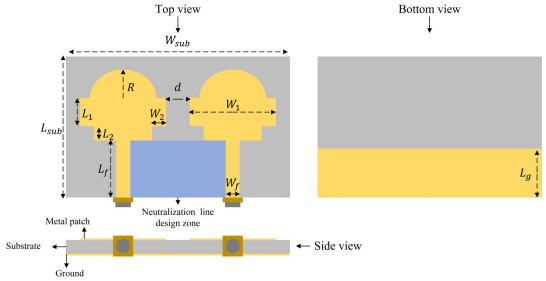

Fig. 4. Structures of the UWB antenna, its substrate is choose as a FR4 substrate with $\varepsilon_r = 4.4$, and loss tangent ($\tan\delta$) $= 0.02$ and thickness $=$ 1.6 mm.

C. Model Training Process

The model training process is divided into two stages: the pretraining stage and the fine-tuning stage. The training process of the model is shown in Fig. 3.

TABLE I
PARAMETERS OF UWB ANTENNA

Parameter	R	L_1	L_2	L_f	L_g	W_1	W_2	W_f	d
Value (mm)	4.8	4.1	3.1	8.5	7.4	14.0	3.5	3.0	4.0

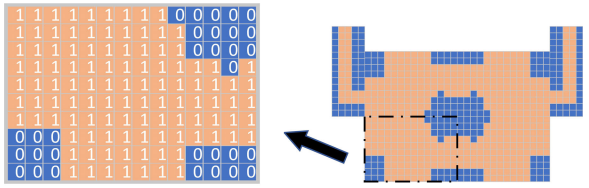

Fig. 5. Generation of neutralization line samples. "1" and "0" represent the presence and absence of metal in the corresponding position, respectively.

The pre-training stage focuses on training the entire model, including the encoder and decoder. Pretraining allows the model to learn the basic mappings. The completed pretrained model can be used for tasks such as classification and reconstruction of samples in the pretrained sample set. However, for an optimization model, on the one hand, we want the model to output better instances than those in the existing sample set. On the other hand, new samples generated during the optimization process are complementary to the existing models and should be fully utilized.

Therefore, the fine-tuning stage focuses on partially tuning the model using the validation samples output by the model during the optimization process that do not meet the design requirements. These new samples are reclassified based on the k-nearest neighbor (k-NN) algorithm, and then the sample dataset is further expanded.

In contrast to the pretraining stage, the fine-tuning only updates the training parameters of the decoder and requires fewer samples and iterations. As the optimization proceeds, the model is simultaneously fine-tuned and its output performance improves.

III. NEUTRALIZATION LINE EXAMPLE

An example of neutralization line design for a two-unit UWB MIMO antenna is used to validate the optimization effect of the proposed method [29]. The geometric structure of the two-element patch antenna with the neutralization line to be optimized is shown in Fig. 4, and its corresponding parameters are listed in Table I.

All the pretrained sample data for the neutralization lines are obtained by the CST software, and all calculations are completed on a Microsoft Windows Server Datacenter workstation with 2× 3.10 GHz Intel Xeon Gold 6248R CPU, Tesla P100-PCIE-16GB GPU, and 1024 GB RAM.

After trading off the number of samples against the required computational resources and time, a total of 3000 pretrained samples of neutralization lines with different middle shapes, line lengths, and widths are obtained using the random generation method and quadrature sampling, as shown in Fig. 5. To further reduce the difficulty of sample generation, prior knowledge is involved. Since the shape positions of the two elements have a high degree of symmetry, the symmetry principle is also applied to the generation of the neutralization line. Besides, based on practical considerations, discrete pixel points are not included. All samples are classified into 50 categories using the k-means algorithm, numbered from 1 to 50, and the larger the digit, the better the isolation performance of the neutralization line within the corresponding category. The parameters involved in the classification include S_{11}, S_{21}, bandwidth, gain, and several other optimization objectives.

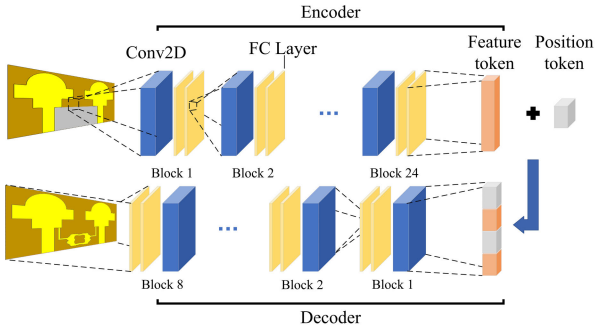

Fig. 6. Detailed MAE architecture.

TABLE II
TRAINING INFORMATION OF MAE NEURAL NETWORK

		Number of epochs/ samples	Time
Sample generation		3000	347.3 h
MAE Training	Pre-train	3000	48.8 h
	Fine-tune	104	1.6 h + 13.8 h (Sim.)

The detailed MAE architecture is shown in Fig. 6, and the activation function is set to GeLU. The training samples are input into the MAE in the form of images, and the resolution is set to 224 × 224. Due to the complexity of MAE and the limited number of samples, much more training samples than test samples are needed to ensure the training effect and avoid falling into mode collapse. Therefore, 2800 samples are randomly selected as training samples and the remaining 200 samples are used as test samples during the pretraining stage of MAE. The number of epochs is set to 3000. The training information of MAE is listed in Table II.

In the fine-tuning stage, since each output gets only one new sample, after the k-NN-based classification of the new sample, all samples within its class and target class are reused for the fine-tuning training. The number of epochs is set to no more than 200.

In each epoch of the fine-tuning, the class label output by the encoder is replaced by the label corresponding to the decoupling structures with the better isolation performance in the sample set, and the corresponding structures are generated by the decoder. When multiple generated structures fail to improve the isolation performance, it indicates that the current structure may have reached the limit of the isolation performance. Therefore, for further optimization, the initial structure is adjusted based on the best existing structure and the masking design area is reselected.

To accomplish the optimization task more efficiently, the design of the neutralization line follows the order of the connecting line and the middle shape. The optimization flow and results of the neutralization line design based on MAE are shown in Fig. 7. The final optimized decoupling structure is simulated by CST. The results show that the neutralization line generated and optimized based on the MAE model has a good decoupling effect. The main function of the 3000 epochs of the pretraining stage is to establish the basic mapping relationship and further clarify the output, and the function of the epochs in the fine-tuning stage is to further adjust the initial structure according to the optimization objective.

IV. MEASUREMENT AND COMPARISON

The antenna is fabricated and measured, and its corresponding results are shown in Figs. 8 and 9. The isolation performance of

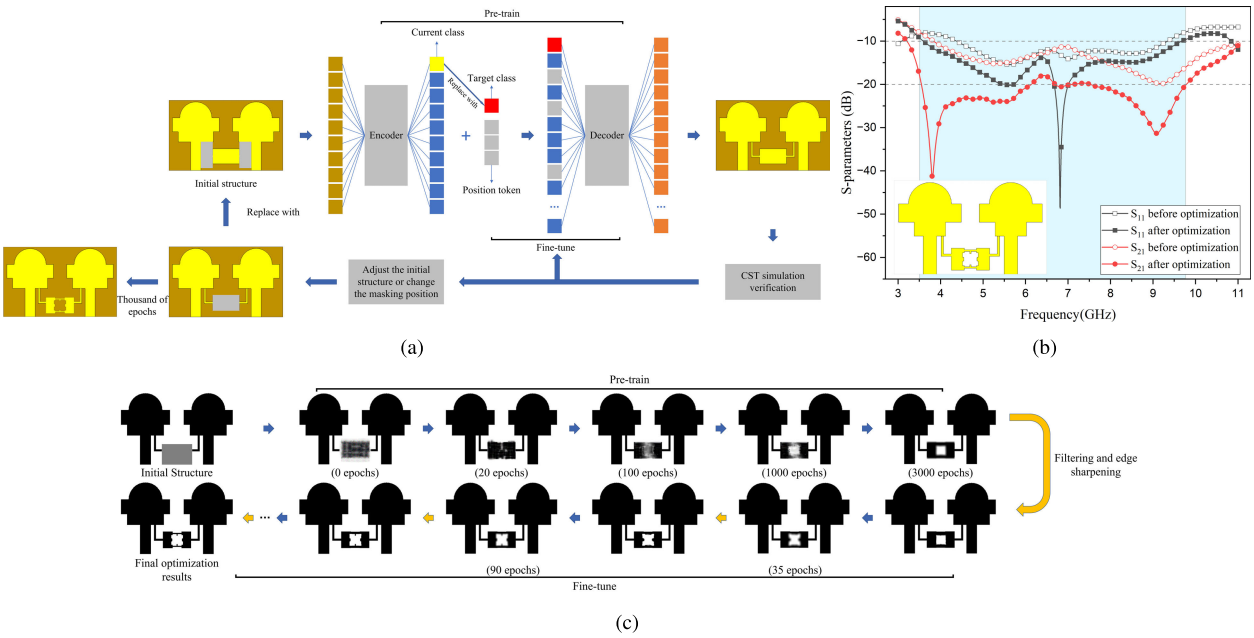

Fig. 7. Flow and results of the design and optimization of the neutralization line based on MAE. (a) Flowchart of the optimization method based on the MAE model, (b) simulation results of neutralization line, and (c) changes of the middle part of neutralization line in the optimization.

TABLE III
COMPARISON INFORMATION WITH SIMILAR OPTIMIZATION ALGORITHMS

References	Optimization method	Optimization objects	Optimization target	Optimization time	Number of simulation samples	Determination of initial stage
[30]	GA	UWB antenna	ultra-wide band response	Not Given	Not Given	trial and error method
[31]		Dual band patch antenna	dual band response			
[32]	GA	Pixel antenna	single S_{11} point	Not Given	8000	number of pixels, general shape of antenna
[33]		Passive metallic reflectors	single E field intensity point	25-30 h	4000	random pixel value, number of pixels
[34]	GA	Transmitarray antenna	magnitude and phase of S_{11} and S_{21}	303.6 h	3645	optimized parameters, random parameter value
[35]	Multi-objective GA	Reconfigurable antenna	beam directions	Not Given	1200	length of genes, number of switches
[36]	GA+CMA	Pixel antenna	modal significance	Not Given	100-200	number of pixels
[37]	GA+SA		S_{11}, radiation pattern	1.7-3.7 h	90-100	trial, monte carlo method
[38]	GP+ANN	Dielectrics around monopole antenna	gain pattern	53 h	1160	random pixel value
This work	MAE+K-means	Neutralization line of UWB antenna	S_{11}, S_{21}, gain	64.2 h	3104	random pixel value, number of pixels

neutralization line designed by MAE reaches below at least −18 dB. The designed neutralization line improves the isolation by at least 6 dB within the whole operating frequency band compared to the antenna without the neutralization line. The simulation results of S_{11} reach below −15 dB between 4.7 and 9.0 GHz, but the practical measurement results have some deterioration (below −10 dB). The measurement results of S_{21} reach below −20 dB, better than the simulation results (−18 dB). The measurement results are basically consistent with the simulation results.

Compared with the initial structure from reference [29], the proposed method not only optimizes the outer shape, but also generates holes inside the shape to get better isolation performance, so it has higher freedom of optimization. During the fine-tuning stage, new samples with better performance are continuously added, and the sample set is in an expanding state, so the model will be more likely to output good neutralization line design.

The proposed optimization method is also compared with some GA-based methods in literature, as listed in Table III.

Compared to the GA-based parametric optimization methods [32], [33], [34], the proposed method has higher freedom of optimization, which can do better local optimization search. The MAE model runs on a pixel-by-pixel basis so it may require more processing time than parametric optimization methods using GA. Compared with the pixel optimization using GA [29], [30], [31], [35], [36], the proposed model has the same flexibility by generating the sample in pixel form. But in the proposed method, prior knowledge can be more easily involved in sample generation, which requires less samples and computational resources. The proposed model is more dependent on the provided

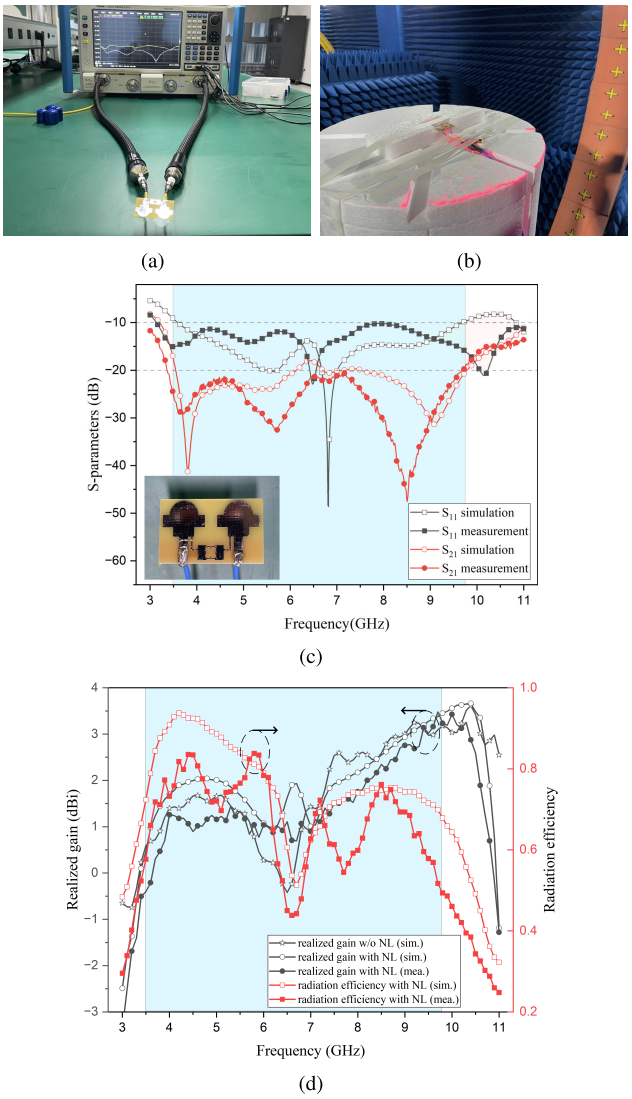

Fig. 8. Measurement results of antenna. (a) measurement of S parameters, (b) measurement of radiation patterns, (c) comparison of S parameters, and (d) comparison of realized gain and radiation efficiency.

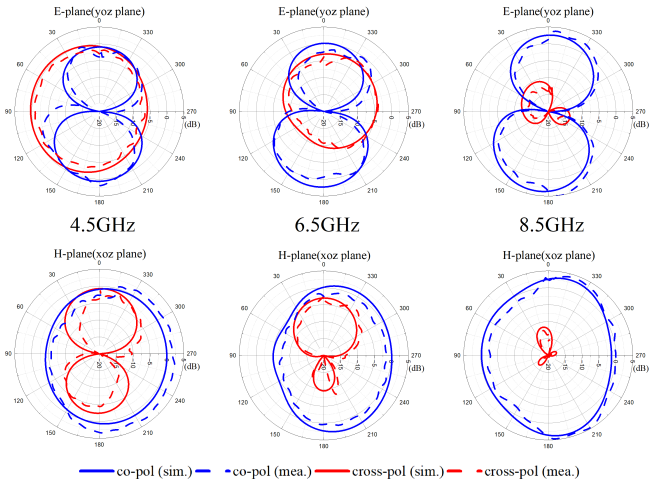

Fig. 9. Simulated and measured radiation pattern.

training samples, and it does not optimize the defined target directly, so it may be more likely to fall into a local optimum than the existing GA-based methods.

V. Conclusion

In this communication, a machine-learning-based optimization method has been proposed to intelligently design neutralization lines. The obtained MAE optimization model can design the masked parts based on the initial structure according to the optimization objectives. An example of neutralization line for UWB antenna is used to validate the effectiveness of the method. About 3000 samples of neutralization lines have been used for the pretraining of MAE. By setting the initial structure of the neutralization lines, the optimization model outputs the required neutralization lines derived from the initial structure and requires little manual intervention of the designer. The measurement results show that the neutralization lines designed by the MAE-based method have good isolation performance within a wide range of frequency bands.

Compared to the parametric optimization models, MAE optimization models can optimize the basic topology of the structure. Compared to the pixel optimization models, it requires less simulation samples. The proposed method can be widely used to passive planar devices, such as metasurfaces, filters, power dividers, and so on.

References

[1] X. Chen, S. Zhang, and Q. Li, "A review of mutual coupling in MIMO systems," *IEEE Access*, vol. 6, pp. 24706–24719, 2018.

[2] S. C. Chen, Y. S. Wang, and S. J. Chung, "A decoupling technique for increasing the port isolation between two strongly coupled antennas," *IEEE Trans. Antennas Propag.*, vol. 56, no. 12, pp. 3650–3658, Dec. 2008.

[3] K. S. Vishvaksenan, K. Mithra, R. Kalaiarasan, and K. S. Raj, "Mutual coupling reduction in microstrip patch antenna arrays using parallel coupled-line resonators," *IEEE Antennas Wireless Propag. Lett.*, vol. 16, pp. 2146–2149, 2017.

[4] X. Tang, X. Qing, and Z. N. Chen, "Simplification and implementation of decoupling and matching network with port pattern-shaping capability for two closely spaced antennas," *IEEE Trans. Antennas Propag.*, vol. 63, no. 8, pp. 3695–3699, Aug. 2015.

[5] C.-H. Wu, C.-L. Chiu, and T.-G. Ma, "Very compact fully lumped decoupling network for a coupled two-element array," *IEEE Antennas Wireless Propag. Lett.*, vol. 15, pp. 158–161, 2016.

[6] S. Shoaib, I. Shoaib, N. Shoaib, X. Chen, and C. G. Parini, "Design and performance study of a dual-element multiband printed monopole antenna array for MIMO terminals," *IEEE Antennas Wireless Propag. Lett.*, vol. 13, pp. 329–332, 2014.

[7] J. Ouyang, F. Yang, and Z. M. Wang, "Reducing mutual coupling of closely spaced microstrip MIMO antennas for WLAN application," *IEEE Antennas Wireless Propag. Lett.*, vol. 10, pp. 310–313, 2011.

[8] L. B. Sun, H. Feng, Y. Li, and Z. Zhang, "Compact 5G MIMO mobile phone antennas with tightly arranged orthogonal-mode pairs," *IEEE Trans. Antennas Propag.*, vol. 66, no. 11, pp. 6364–6369, Nov. 2018.

[9] C.-D. Xue, X. Y. Zhang, Y. F. Cao, Z. Hou, and C. F. Ding, "MIMO antenna using hybrid electric and magnetic coupling for isolation enhancement," *IEEE Trans. Antennas Propag.*, vol. 65, no. 10, pp. 5162–5170, Oct. 2017.

[10] S. Zhang and G. F. Pedersen, "Mutual coupling reduction for UWB MIMO antennas with a wideband neutralization line," *IEEE Antennas Wireless Propag. Lett.*, vol. 15, pp. 166–169, 2016.

[11] J. Wang, X.-S. Yang, X. Ding, and B.-Z. Wang, "Antenna radiation characteristics optimization by a hybrid topological method," *IEEE Trans. Antennas Propag.*, vol. 65, no. 6, pp. 2843–2854, Jun. 2017.

[12] X. S. Yang, K. T. Ng, S. H. Yeung, and K. F. Man, "Jumping genes multiobjective optimization scheme for planar monopole ultrawideband antenna," *IEEE Trans. Antennas Propag.*, vol. 56, no. 12, pp. 3659–3666, Dec. 2008.

[13] F. Jiang, C. Chiu, S. Shen, Q.-S. Cheng, and R. Murch, "Pixel antenna optimization using N-port characteristic mode analysis," *IEEE Trans. Antennas Propag.*, vol. 68, no. 5, pp. 3336–3347, May 2020.

[14] B. Liu, H. Aliakbarian, Z. Ma, G. A. E. Vandenbosch, G. Gielen, and P. Excell, "An efficient method for antenna design optimization based on evolutionary computation and machine learning techniques," *IEEE Trans. Antennas Propag.*, vol. 62, no. 1, pp. 7–18, Jan. 2014.

[15] J. E. Rayas-Sanchez, "EM-based optimization of microwave circuits using artificial neural networks: The state-of-the-art," *IEEE Trans. Microw. Theory Techn.*, vol. 52, no. 1, pp. 420–435, Jan. 2004.

[16] Y. Sharma, H. H. Zhang, and H. Xin, "Machine learning techniques for optimizing design of double T-shaped monopole antenna," *IEEE Trans. Antennas Propag.*, vol. 68, no. 7, pp. 5658–5663, Jul. 2020.

[17] S. Han, Y. Tian, W. Ding, and P. Li, "Resonant frequency modeling of microstrip antenna based on deep kernel learning," *IEEE Access*, vol. 9, pp. 39067–39076, 2021.

[18] G. Angiulli, M. Cacciola, and M. Versaci, "Microwave devices and antennas modeling by support vector regression machines," *IEEE Trans. Magn.*, vol. 43, no. 4, pp. 1589–1592, Mar. 2007.

[19] L. Yuan, L. Wang, X.-S. Yang, H. Huang, and B.-Z. Wang, "An efficient artificial neural network model for inverse design of metasurfaces," *IEEE Antennas Wireless Propag. Lett.*, vol. 20, no. 6, pp. 1013–1017, Jun. 2021.

[20] Z. Wei and X. Chen, "Physics-inspired convolutional neural network for solving full-wave inverse scattering problems," *IEEE Trans. Antennas Propag.*, vol. 67, no. 9, pp. 6138–6148, Sep. 2019.

[21] R. Guo et al., "Solving combined field integral equation with deep neural network for 2-D conducting object," *IEEE Antennas Wireless Propag. Lett.*, vol. 20, no. 4, pp. 538–542, Apr. 2021.

[22] H. M. Yao and L. Jiang, "Machine-learning-based PML for the FDTD method," *IEEE Antennas Wireless Propag. Lett.*, vol. 18, no. 1, pp. 192–196, Jan. 2019.

[23] K. He, X. Chen, S. Xie, Y. Li, P. Dollár, and R. Girshick, "Masked autoencoders are scalable vision learners," 2021, *arXiv:2111.06377*.

[24] A. Torralba, R. Fergus, and Y. Weiss, "Small codes and large image databases for recognition," in *Proc. IEEE Conf. Comput. Vis. Pattern Recognit.*, Jun. 2008, pp. 1–8.

[25] P. Vincent, H. Larochelle, Y. Bengio, and P. M. Dept, "Extracting and composing robust features with denoising autoencoders," in *Proc. 25th Int. Conf. Mach. Learn.*, Feb. 2008, pp. 1096–1103.

[26] G. E. Hinton and R. R. Salakhutdinov, "Reducing the dimensionality of data with neural networks," *Science*, vol. 313, no. 5786, pp. 504–507, 2006.

[27] A. Krizhevsky and G. E. Hinton, "Using very deep autoencoders for content-based image retrieval," in *Proc. Eur. Symp.*, 2012, pp. 1–12.

[28] Z.-H. Zhou, *Machine Learning*. Beijing, China: Tsinghua Univ. Press, 2016.

[29] R. N. Tiwari, P. Singh, B. K. Kanaujia, and K. Srivastava, "Neutralization technique based two and four port high isolation MIMO antennas for UWB communication," *AEU-Int. J. Electron. Commun.*, vol. 110, Oct. 2019, Art. no. 152828.

[30] M. C. Derbal, A. Zeghdoud, and M. Nedil, "A novel UWB antenna for wireless communication systems using genetic algorithms," in *Proc. IEEE Int. Symp. Antennas Propag. USNC-URSI Radio Sci. Meeting*, Atlanta, GA, USA, Jul. 2019, pp. 1095–1096.

[31] M. C. Derbal, A. Zeghdoud, and M. Nedil, "A novel dual band antenna design for WiFi applications using genetic algorithms," in *Proc. IEEE Int. Symp. Antennas Propag. USNC/URSI Nat. Radio Sci. Meeting*, Boston, MA, USA, Jul. 2018, pp. 1009–1010.

[32] G. C. Karaova and O. Ergul, "Design, fabrication, and measurement of efficient beam-shaping reflectors for 5G applications," *IEEE Trans. Antennas Propag.*, vol. 70, no. 12, pp. 11335–11343, Dec. 2022.

[33] S. Guler, B. Karaosmanoglu, and O. Ergul, "Design, simulation, and fabrication of a novel type of inkjet-printed pixel antennas," *Prog. Electromagn. Res. Lett.*, vol. 64, pp. 51–55, 2016.

[34] X. Liu et al., "Ultrabroadband all-dielectric transmitarray designing based on genetic algorithm optimization and 3-D print technology," *IEEE Trans. Antennas Propag.*, vol. 69, no. 4, pp. 2003–2012, Apr. 2021.

[35] X. Yuan et al., "A parasitic layer-based reconfigurable antenna design by multi-objective optimization," *IEEE Trans. Antennas Propag.*, vol. 60, no. 6, pp. 2690–2701, Apr. 2012.

[36] F. Jiang et al., "Multiport pixel antenna optimization using characteristic mode analysis and sequential feeding port search," *IEEE Trans. Antennas Propag.*, vol. 70, no. 10, pp. 9160–9174, Oct. 2022.

[37] F. Jiang et al., "Pixel antenna optimization based on perturbation sensitivity analysis," *IEEE Trans. Antennas Propag.*, vol. 70, no. 1, pp. 472–486, Jul. 2022.

[38] Y. Sharma, X. Chen, J. Wu, Q. Zhou, H. H. Zhang, and H. Xin, "Machine learning methods-based modeling and optimization of 3-D-printed dielectrics around monopole antenna," *IEEE Trans. Antennas Propag.*, vol. 70, no. 7, pp. 4997–5006, Jul. 2022.